REPORT DOCUMENTATION PAGE

Form Approved
OMB No. 0704-0188

1. REPORT DATE *(DD-MM-YYYY)*	2. REPORT TYPE	3. DATES COVERED *(From - To)*
11/15/2013	Interim Research Performance Report	06/1/2012 - 08/31/2013

4. TITLE AND SUBTITLE
Interim Research Performance Report
Quarterly Report No. 8

5a. CONTRACT NUMBER

5b. GRANT NUMBER
N00014-11-1-0752

5c. PROGRAM ELEMENT NUMBER

6. AUTHOR(S)
Nathan E. Murray, Charles E. Tinney (U. of Texas at Austin), Brian S. Thurow (Auburn Univ.), Praveen Panickar (CRAFT Tech.)

5d. PROJECT NUMBER

5e. TASK NUMBER

5f. WORK UNIT NUMBER

7. PERFORMING ORGANIZATION NAME(S) AND ADDRESS(ES)
The University of Mississippi
Jamie Whitten National Center for Physical Acoustics
University, MS 38677

8. PERFORMING ORGANIZATION REPORT NUMBER

9. SPONSORING/MONITORING AGENCY NAME(S) AND ADDRESS(ES)
Joseph Doychak
Office of Naval Research
875 North Randolph Street
Arlington, VA 22203-1995

10. SPONSOR/MONITOR'S ACRONYM(S)
ONR

11. SPONSOR/MONITOR'S REPORT NUMBER(S)

12. DISTRIBUTION/AVAILABILITY STATEMENT
Approved for Public Release; Distribution is Unlimited

13. SUPPLEMENTARY NOTES

14. ABSTRACT
The research team completed remaining work on the base effort including post-processing of the Plenoptic PIV data and compilation of the non-linear propagation work. Following the peer review, the original work plan for the extension period was determined to be too broad in scope. Therefore, a new extension work plan with reduced scope was proposed.

15. SUBJECT TERMS
Jet Noise Reduction, High Dynamic Range PIV, Computational Phased Array Beamforming, Aeroacoustics

16. SECURITY CLASSIFICATION OF:			17. LIMITATION OF ABSTRACT	18. NUMBER OF PAGES	19a. NAME OF RESPONSIBLE PERSON
a. REPORT	b. ABSTRACT	c. THIS PAGE		22	Nathan E. Murray
					19b. TELEPHONE NUMBER *(Include area code)* 662-915-3190

Toward Active Control of Noise
from Hot Supersonic Jets

Quarterly Progress Report No. 8

1 June 2013 – 31 August 2013

Nathan E. Murray (PI)
National Center for Physical Acoustics
The University of Mississippi
University, MS 38677
(662) 915-3190
nmurray@olemiss.edu

Charles E. Tinney (Co-PI) – The University of Texas at Austin
Brian S. Thurow (Co-PI) – Auburn University
Praveen Panickar – Combustion Research and Flow Technology, Inc.

Contract: N00014-11-1-0752

Attn: Joseph Doychak & Brenda Henderson
Office of Naval Research
Arlington, VA 22203-1995
joseph_doychak@onr.mil | brenda.s.henderson@navy.mil

Executive Summary

The research team completed remaining work on the base effort including post-processing of the Plenoptic PIV data and compilation of the non-linear propagation work. Following the peer review, the original work plan for the extension period was determined to be too broad in scope. Therefore, a new extension work plan with reduced scope was proposed.

15 November 2013

Contents

1 Project Objectives and Status

1.1 Review of Program Objectives

The base effort was intended to address the deficiency in the understanding of the effect that near-nozzle and inner-nozzle flow conditions have on jet noise radiation. There were three primary objectives:

1. high-fidelity characterization of heated, over-expanded supersonic jets,
2. source identification through development of advanced analytical diagnostics, and
3. enhanced computational modeling of hot supersonic jets.

1.2 Project Status

This reporting period marks the end of the base effort. Figure 1 shows the project status. The following list summarizes completion/incompletion of specific WBS entries.

WBS 1.4 The methodology for computation of the relevant terms was completed using data generated from the LES (large-eddy simulation) in WBS 2.3. These results were presented at the 2013 AIAA/CEAS Aeroacoustics conference as papers 2013-2081 and 2013-2193.

WBS 2.1.4 The temperature profile measurements were not completed. The first attempt ended due to probe failure. Focus on the MHz rate measurements in WBS 2.2.2 took presedence and we did not revisit these measurements.

WBS 2.2.2 The campaign was completed, but the measurements were less successful than anticipated. Details are discussed in Section 2.2.

WBS 3.0 The main deficiencies with the experimental measurements were related to the Cordin camera: misalignment of the individual MCP (multi-channel plate) units and resonant vibration of the pellicle beam splitters. Neither of these problems could be rectified in the lab. As a result, we could not complete the related data analysis. Efforts to extract at least some velocity data are being conducted by Dr. Thurow's graduate student, Bryan Brock, and will be presented at the upcoming AIAA SciTech Conference.

WBS 5.0 Plenoptic PIV data was acquired to attempt a different method of flow field measurement. Results and suggestions for future work are discussed in Section 2.2.

WBS 6.0 The phase-array methodology was completely implemented and results were presented at the peer review.

WBS 8.0 This report completes the quarterly reporting in the base period.

WBS 9.0 A final report is not required at this time as a no-cost extension has been granted in connection with the project extension.

WBS 10.2 The year 2 peer review was completed. Reviewer comments led to a proposed reduction in scope for the year 3 project extension.

1.3 Extension Proposal

Given the lack of progress on the time-resolved flow-field measurements, we were encouraged to propose a modified work plan for a contract extension that focused on the near-field propagation of jet noise. The extension work will address two question.

1. Do the shock-like structures form inside the jet flow or are they the result of rapid steepening immediately outside of the jet?

2. What is the correct decay law for the acoustic signature?

The extension proposal was submitted on 16 September 2013 with the project plan shown in Figure 2

2 Activity for Current Reporting Period

2.1 Jet Acoustics and Crackle

The progress on the non-linear propagation work was compiled and summarized in Woutijn Baars's dissertation under the direction of Dr. Tinney. The summary is provided in Appendix A. The summary also provide suggestions for future work that are relevant to our efforts moving forward in the extension period of this program.

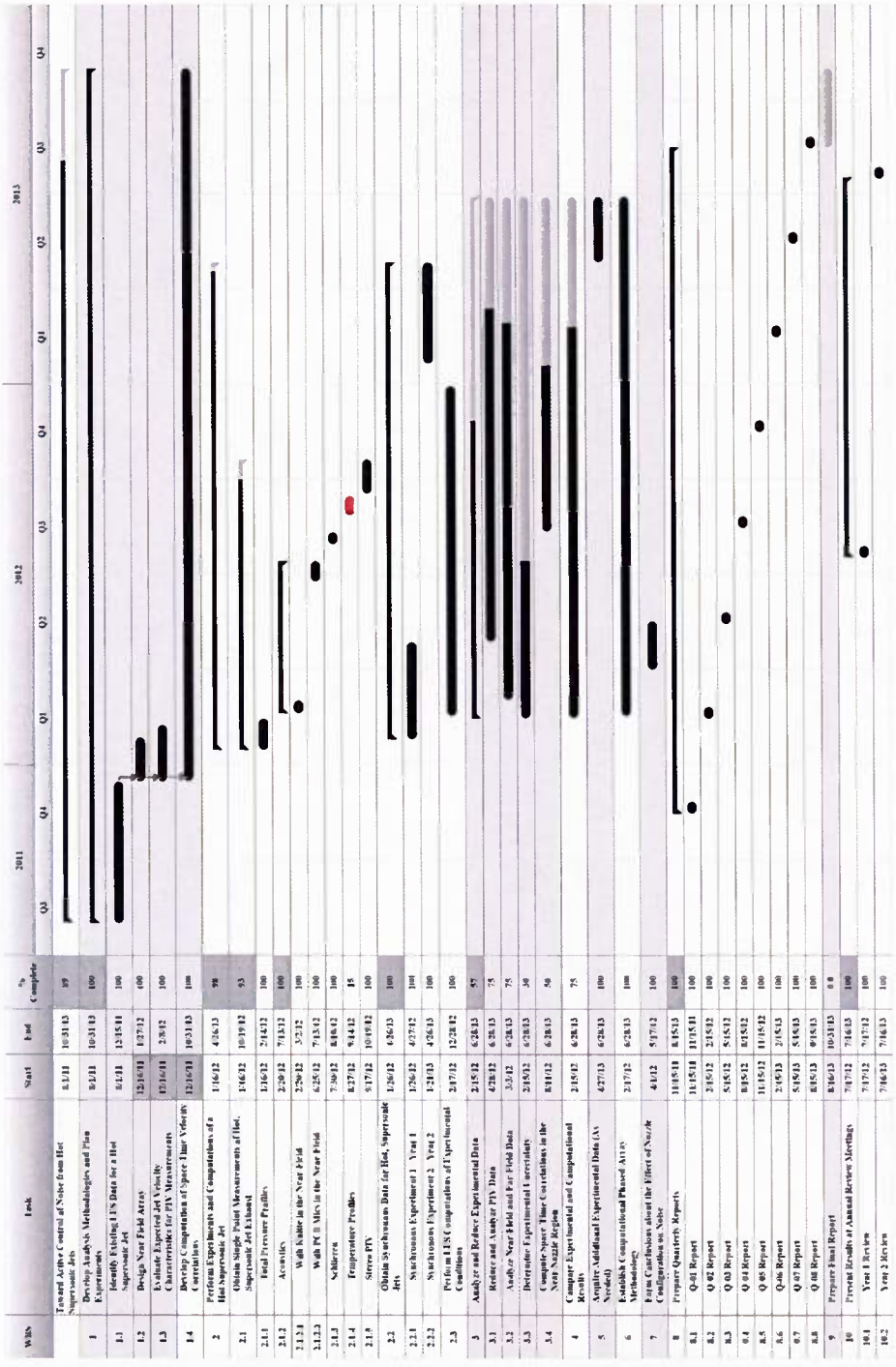

Figure 1. Project chart showing WBS items and current completion status as of the end of the reporting period.

	Extension Work Period			
1 Oct 2013 – 30 September 2014	Q4	Q1	Q2	Q3
WBS 1.0 Determine Amplitude and Decay Rate of Acoustic Waveform	■	■		
WBS 1.1 Separating hydrodynamic and acoustic components of the wave form.	■	■		
WBS 1.2 Conduct measurements on a Mach 3 shock-free jet using 1/8-inch microphones.	■			
WBS 1.3 Develop Gol'dburg numbers for jet noise problems.		■	■	
WBS 1.4 Demonstrate and validate the decay law model with acoustic data from hot, shock-containing jets.			■	■
WBS 2.0 Prepare Quarterly Reports	✓	✓	✓	✓
WBS 3.0 Present Results at Annual Review Meeting			✓	
WBS 4.0 Prepare Final Report				✓

Figure 2. Extension work plan.

2.2 High-Fidelity Flow Field Measurements

2.2.1 Time-Resolved PIV: Lessons Learned

As indicated in the review of the base effort and evidenced in our annual reports, progress with time-resolved PIV has been slow and frustrating. In the first year, a combination of poor particle seeding and poor image quality stifled progress. In the second year, particle seeding issues were overcome; however, the image quality and slow acquisition rate of the Cordin camera severely hampered progress and limited acquisition to a single set of data (over 300 image sequences were acquired and are currently being processed). As such, the vast majority of the data processing effort has been the development of image processing algorithms to overcome these issues as opposed to exploiting the unique information afforded by this system. Unfortunately, these issues have prevented us from proceeding on to more interesting aspects such as asynchronous triggering.

2.2.2 Plenoptic PIV: A Different Experience than Time-Resolved PIV

In the 2nd year of the base effort we conducted a simple proof-of-concept experiment in the NCPA facility with a plenoptic camera designed and built by co-PI Thurow to test the feasibility of performing 3D velocity measurements in a heated supersonic jet. In stark contrast to the experience with time-resolved PIV, the experience with the plenoptic camera went very smoothly as we were able to acquire over 300 image pairs in 1 day of testing without any major issues. This included both the time to set-up the experiments as well as acquire the data. As will be detailed below, this simple proof-of-concept experiment yielded good quality data that reveals details about the large-scale 3D structure of the jet flow.

Figure 3. Illustration of ability to computational refocus an image after it has been acquired.

2.2.3 Plenoptic PIV: Background and Sample Results

As plenoptic PIV was not part of the originally proposed effort, a brief background of the technique is provided here. More details are available in [1, 2, 3, 4, 5]. A plenoptic camera is distinguished from a conventional camera in its unique ability to record the 4D light-field of a scene. The term light-field describes the complete distribution of light rays in space leading to a 4D function, sometimes termed the plenoptic function, wherein each light ray is characterized by its position (x, y) on a plane and its propagation angle (θ, ϕ). Standard imaging captures only two dimensions of the 4D light-field as angular information is integrated at the sensor's surface, leading to familiar imaging phenomena such as de-focus, depth-of-field and image blur. A plenoptic camera, on the other hand, uses a microlens array placed near a conventional image sensor to measure both the position and angle of light rays captured by the camera lens, thus forming a 4D measurement of the light-field. Co-PI Thurow has recently designed and assembled a plenoptic camera in his laboratory with its key attributes being its compact size, simple design, ease of operation and ability to collect light-field data in a single snapshot. Figure 3 illustrates one of the many uses of light-field data: the ability to computationally refocus an image after acquisition. These images were computed from a single snapshot using an in-house ray-tracing algorithm to virtually propagate the light rays forward and backward in space, and integrate the angular information in a manner similar to a conventional camera. This refocusing feature is the most noteworthy aspect of the consumer camera developed by Lytro Inc. with variations of this technology also available from Raytrix. Another common use of the data is to generate views obtained with different perspectives. With our camera, we are able to generate over 100 unique views from different angles from a single snapshot of data.

The emphasis of Co-PI Thurow's work over the last three years has been on adaptation of this technology for 3D velocity measurements. This has included development of both the hardware and software necessary to realize 3D velocity measurements in a turbulent flow. The first experimental demonstration of the camera focused on the collection of plenoptic PIV image data in both ZPG (zero pressure gradient) and APG adverse pressure gradient turbulent boundary layers ($Re_\theta = 4,500$ and $7,200$, respectively). To determine the full 3D/3C velocity field, a pair of 3D particle fields were reconstructed from individual snapshots of the light-field data using limited-angle tomography algorithms (the MART algorithm used in tomo-PIV). Conventional 3D PIV cross-correlation algorithms were then applied to the particle volumes to determine the particle displacement and velocity. Examples of other flows in which the plenoptic camera's capabilities have been demonstrated are the aforementioned turbulent boundary layers, visualization of the counter-rotating vortices generated by

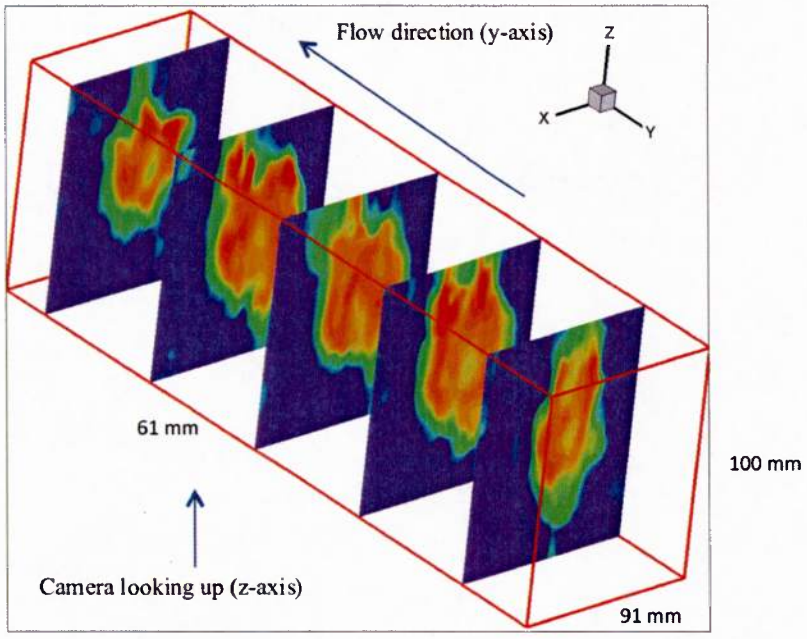

Figure 4. Sample 3D velocity field obtained in a 2″ diameter supersonic jet seeded with alumina particles. Y-axis is stretched by a factor of 5 to illustrate different cross-sections of the jet. Color corresponds to streamwise, u_y, component of velocity.

a Wheeler doublet vortex tab in a turbulent boundary layer and the supersonic jet results discussed here.

Figure 4 shows an example of the data recently acquired in the NCPA demonstration. It is an instantaneous 3D/3C (3-dimensional/3-component) velocity field obtained in the heated, supersonic jet at the center of this study. The jet Mach number was 1.74, the total temperature ratio was 3.37 and the jet diameter 50.8 mm. The dimensions of the volume are approximately 100 x 91 x 66 mm centered approximately 1.5 jet diameters downstream from the nozzle exit. The volume was illuminated with a 200 mJ/pulse PIV laser and the camera was mounted approximately 18" away from the jet. Particle seeding was obtained in the same fashion as previous PIV experiments using alumina particles suspended in ethanol and injected into the jet's settling chamber. All calculations were performed on a standard desktop computer.

A selection of image pairs from the November 2012 effort were analyzed. A subset of 24 image pairs were processed and used to determine mean and rms quantities. Figure 5(a) shows the average velocity field calculated from this limited set of data. A key feature of the average velocity field is the presence of a low velocity region in the center of the jet resulting from the slipline where shocks converge. This matches probe measurements and computational simulations. Other features, such as the relatively thin shear layer and magnitude of the velocity is also consistent with expectations. Figure 5(b) shows the RMS fluctuations of the velocity field. The jet core and ambient both show low levels of fluctuations whereas the shear layer shows the highest levels of fluctuations. The key point is that

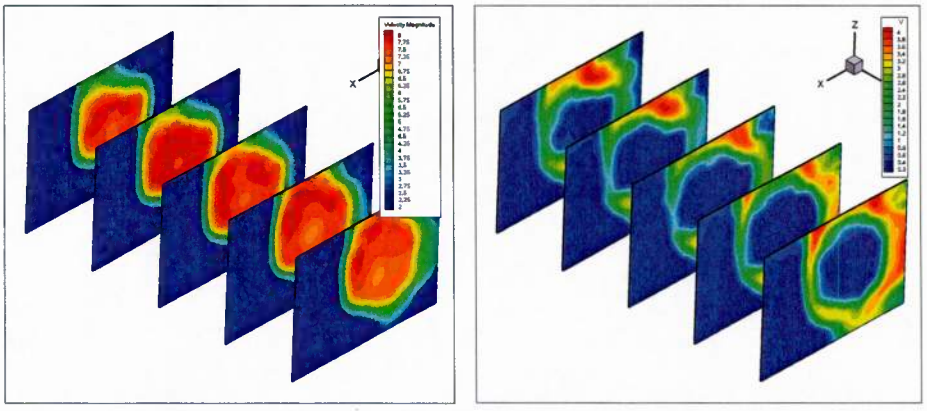

(a) Mean Velocity Field (b) RMS Velocity Fluctuations

Figure 5. Average and RMS velocities calculated using 24 image pairs. Five cross-sections are shown with the lower velocity jet core apparent near the center of the jet. Velocity scale ranges from 200 (blue) to 800 (red) m/s.

plenoptic PIV accurately shows the three dimensional location where velocity fluctuations are known to occur.

2.2.4 Plenoptic PIV: Comment on Occlusions

A concern was expressed about how the plenoptic PIV technique can overcome occlusions, presumably due to the notion that particles will obstruct the view of other particles. We do not believe this to be a problem for the following reasons. In principle, for very low image densities where particles can be explicitly identified, the 3D location of a particle can be determined using only two images acquired from different viewing angles, such as achieved commonly in particle tracking velocimetry experiments. For higher image densities where individual particles cannot be explicitly identified, tomo-PIV has recently emerged as a viable technique for 3D flow measurements. In tomo-PIV, tomographic algorithms are used to reconstruct a volume of particles based on 2D projections (e.g. images) of the volume onto cameras located at different angular positions around the volume. In this configuration occlusions are still present for some of the views; however, the additional views provide enough additional information for the tomographic algorithms to accurately reconstruct the location of particles within the volume. The effect of occlusions is a reconstruction artifact known as 'ghost particles' that degrades the quality of the reconstruction. It was found that the influence of ghost particles decreases significantly as one increases the number of cameras in the system, with four cameras considered reasonable for many applications. We do not believe plenoptic PIV is affected by this problem because, in the context of the above description, the plenoptic camera produces the virtual equivalent of *over 100 distinct projections of the volume.* We have tested this using a synthetic image generator developed specifically for particle imaging with a plenoptic camera. Figure 6 shows the reconstruction quality, Q, as a function of the particle number density. In this case, the number of pixels is taken as the total number of active pixels on the camera which is equal to 11×106. As

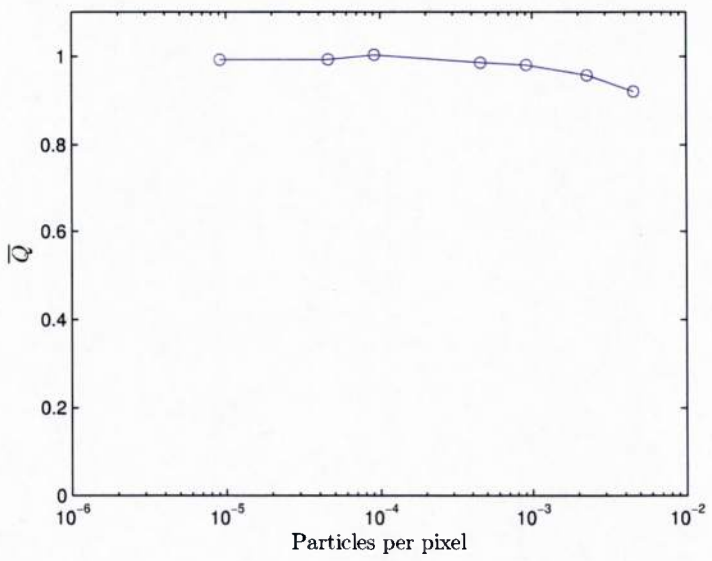

Figure 6. Reconstruction quality as a function of number of particles. Particles per pixel are calculated based on the total number of active pixels on the camera (11×106 **pixels).**

can be seen, the quality of the reconstruction is relatively flat over a large range of particle number densities and exhibits a graduate decrease for large particle number densities. As such, we believe plenoptic PIV is fairly robust and resistant, particularly in comparison to techniques such as tomo-PIV.

Along the same lines, plenoptic PIV affords additional advantages over tomo-PIV that make it well suited for this study. Typical tomo-PIV systems are limited to relatively thin (order 10 mm thick) volumes partially to limit the particle number density of the projections, but also to satisfy the requirement that the full volume remain within the depth-of-field of each camera. To achieve this, each camera lens is typically adjusted to a small aperture setting to increase the depth-of-field. This significantly limits the amount of light collected by the camera, further restricting the size of the volume due to the need for very high energy laser pulse illumination. Plenoptic PIV, on the other hand, avoids these complications as it does not require the volume to be "in-focus" in a conventional sense. Rather, plenoptic PIV actually works better with a wide open aperture due to the increased angular content sampled by the camera. This was illustrated by the November 2012 NCPA acquisition under the base effort where a conventional PIV laser provided sufficient illumination. Combined with the mitigation of ghost particles, plenoptic PIV is well suited for 3D measurements of 'thick' volumes.

[1] FAHRINGER, T. & THUROW, B. (2012) "Tomographic Reconstruction of a 3-D Flow Field Using a Plenoptic Camera," in *42nd AIAA Fluid Dynamics Conference* (New Orleans, LA).

[2] FAHRINGER, T. & THUROW, B. (2013) "The Effect of Grid Resolution on the Accuracy of Tomographic Reconstruction Using a Plenoptic Camera," in *51st AIAA Aerospace Sciences Meeting.*

[3] LYNCH, K. (2011) *Development of a 3-D Fluid Velocimetry Technique Based on Light Field Imaging*, Master's thesis, Auburn University.

[4] LYNCH, K., FAHRINGER, T. & THUROW, B. (2012) "Three-Dimensional Particle Image Velocimetry Using a Plenoptic Camera," in 50^{th} *AIAA Aerospace Sciences Meeting*, 2012-1056 (AIAA, Nashville, TN).

[5] THUROW, B. & FAHRINGER, T. (2013) "Recent Development of Volumetric PIV with a Plenoptic Camera," in 10^{th} *International Symposium on Particle Image Velocimetry* (Delft, Netherlands).

3 Technical/Cost Status & Problem Areas

The application of MHz PIV to the high-noise environment near the jet proved a technical challenge that could not overcome in the present work. As a result, the extension work plan was reduced to focus on the propagation of the high amplitude jet noise acoustics.

4 Publications, Meetings, and/or Travel

4.1 Running List of Publications Produced

[1] BAARS, W.J., TINNEY, C.E., MURRAY, N.E., JANSEN, B.J. & PANICKAR, P. (2011) "The Effect of Heat on Turbulent Mixing Noise in Supersonic Jets," in 49^{th} *AIAA Aerospace Sciences Meeting*, Paper 2011-1029 (Orlando, FL).

[2] BAARS, W.J., TINNEY, C.E. & WOCHNER, M.S. (2012) "Nonlinear Noise Propagation from a Fully Expanded Mach 3 Jet," in *50th AIAA Aerospace Science Meeting*, Paper 2012-1177 (Nashville, TN).

[3] MURRAY, N.E., LYONS, G.W., TINNEY, C.E., DONALD, B., BAARS, W.J., THUROW, B.S., HAYNES, R.H. & PANICKAR, P. (2012) "A Laboratory Framework for Synchronous Near/Far-Field Acoustics and MHz PIV in High-Temperature, Shock-Containing, Jets," in *Proceedings of the Internoise 2012/ASME NCAD Meeting*, ASME/NCAD-1270 [invited] (New York City, NY).

[4] BAARS, W.J. & TINNEY, C.E. (2012) "Scaling Model for Nonlinear Supersonic Jet Noise," in *Bulletin of the American Physical Society*, **57**:17, Abstract D24:8 (San Diego, CA).

[5] PANICKAR, P., ERWIN, J., SINHA, N., MURRAY, N.E. & LYONS, G.W. (2013) "Localization of Acoustic Sources in Shock-Containing Jet Flows Using Phased Array Measurements," in 51^{st} *AIAA Aerospace Sciences Meeting*, 2013-0613 (Grapevine, TX).

[6] HAYNES, R.H., BROCK, B.A. & THUROW, B.S. (2013) "Application of MHz Frame Rate, High Dynamic Range PIV to a High-Temperature, Shock-Containing Jet," in 51^{st} *AIAA Aerospace Sciences Meeting*, 2013-0774 (Grapevine, TX).

[7] FIÉVET, R., TINNEY, C.E., MURRAY, N.E., LYONS, G.W. & PANICKAR, P. (2013) "Acoustic Source Indicators using LES in a Fully Expanded and Heated Supersonic Jet," in 19^{th} *AIAA/CEAS Aeroacoustics Conference*, 2013-2193 (Berlin, Germany).

[8] BAARS, W.J. & TINNEY, C.E. (2013) "Quantifying Crackle-Inducing Acoustic Shock-Structures Emitted by a Fully-Expanded Mach 3 Jet," in *19th AIAA/CEAS Aeroacoustics Conference*, Paper 2013-2081 (Berlin, Germany).

[9] BAARS, W.J. & TINNEY, C.E. (2013) "A Temporal and Spectral Quantification of the Crackle Component in Supersonic Jet Noise," in *2nd Symposium on Fluid-Structure-Sound Interactions and Control*, p. 170 (Shatin, Hong Kong).

[10] BAARS, W.J., TINNEY, C.E. & WOCHNER, M.S. "Nonlinear Distortion of Acoustic Waveforms from High-Speed Jets," *J. of Fluid Mechanics* [in review].

[11] BAARS, W.J. (2013) *Acoustics from High-speed Jets with Crackle*, Ph.D. Dissertation, The University of Texas at Austin.

5 Planned Activities for Next Reporting Period

- Initiate work under the project extension and complete all related subcontract modifications.
- Extract a data set from the LES with more samples and a larger spatial domain than used previously for analysis under the project extension.
- Conduct measurements on a Mach 3 shock-free jet using 1/8-inch microphones.

Appendix A: Excerpt: "Summary and Future Work," from *Acoustics from High-Speed Jets with Crackle* by Woutijn Baars

Chapter 7

Summary and future work

The summary is condensed into two parts. At first, the research on cumulative nonlinear waveform distortions in the acoustic field of high-speed jets is reviewed (§ 7.1). Secondly, the investigation of crackle-inducing signatures is summarized in § 7.2. Suggestions for future work are itemized throughout the summary.

7.1 Cumulative nonlinear waveform distortions

The acoustic field of an unheated and perfectly expanded Mach 3 experimental jet was examined to understand the degree of both local and cumulative nonlinear distortions of waveforms emitted by high-speed jets. The source mechanisms of interest are those that are known to produce Mach waves, which become pronounced as the convective speed of the large-scale events in the shear layer move at supersonic speeds relative to the ambient surroundings. Most intense noise is emitted from a region bounded by the potential core and the point of sonic velocity on the jet's centerline. The resultant sound field forms a highly directive pattern with a ridge that follows along the Mach cone half angle of the jet.

A model for predicting the presence of cumulative nonlinear effects, distorting acoustic waveforms produced by jet flows, was then proposed. The model considers the broadband sound along the peak noise path and is based on an assessment of the effective Gol'dberg number: a ratio of shock formation distance to acoustic absorption length. Relevant scaling parameters are shown to comprise Mach number (gas dynamic or acoustic), temperature ratio, and Strouhal number corresponding to the peak frequency of the broadband noise. The model assumes that the noise is emitted from a location that scales with nozzle diameter. Model predictions are justified by several laboratory- and full-scale data sets. Two different scaling scenarios are presented for the practising scientist to choose from. The first of these allows shock formation distance to be preserved between laboratory and full-scale conditions and is based on a scaling of the shock formation distance to nozzle diameter. The second scenario allows one to preserve the wave steepening process between laboratory and full-scale conditions based on a match of the effective Gol'dberg number. Both methods provide promising results upon application of the laboratory and full-scale experimental data sets. There are, of course, opportunities to improve the model; these are proposed in itemized form.

- A more thorough assessment of how jet exit conditions affect scaling parameters has to be pursued. Where Strouhal number is concerned, it is still unclear how the peak frequency along the peak noise propagation path depends on jet exit conditions such as temperature ratio or Mach number. It is also assumed here that the location from where

the waveform is emitted scales with nozzle diameter only. This assumption disregards the dependence of the emission-point location on Mach number, Reynolds number, temperature ratio, or even the operating state of the nozzle (overexpanded or underexpanded). Deficiencies in the understanding of these dependencies would be alleviated by accurate parametrization of the effects of Strouhal number, Mach number, temperature ratio, and Reynolds number on the emission-point location of the broadband noise that is an input to the model. Taking the effect into account of jets operating at overexpanded or underexpanded conditions are of great practical significance to this. For off-design conditions, broadband shock noise is saturated by turbulent mixing noise along shallow angles to the jet axis (within the Mach cone of the jet) so distortions to the acoustic waveform are still anticipated so long as the effective Gol'dberg number is shown to be sufficiently large.

- It is unclear to what effect a pre-steepened acoustic waveform has on shock formation distance. Waveform steepening occurs when the wave amplitude is large enough to overcome viscous absorption. This requires a large source intensity and hence, a high Mach number at the exit. This suggests that cumulative nonlinear acoustic distortions are unlikely to occur under subsonic jet exit conditions. Albeit, viscous absorption is considerably weaker at low frequencies, and so it is still plausible for a geometrically large subsonic flow to produce acoustic waves capable of undergoing cumulative nonlinear distortions. Nevertheless, Mach waves

that develop in supersonic jet flows produce pre-steepened waveforms at the source which can accelerate the wave steepening process and shorten the shock formation distance. A carefully documented execution of the generalized Burgers equation using pre-steepened waveforms could provide some useful answers to this concern.

- Currently, the model computes the shock formation distance of the broadband noise as if the sound pressure along the peak noise path obeys by spherical spreading ($p \propto 1/\rho$). However, in close vicinity to the emission-point location, the sound pressure decays cylindrically ($p \propto 1/\sqrt{\rho}$) due to the non-compact nature of the noise sources. And so, when taking that into account accordingly, the shock formation distance will increase. However, a pre-steepened waveform, addressed in the previous point, will result in a shorter shock formation distance.

Temporal waveforms from the Mach 3 jet were examined using various statistical (ensemble-averaged) metrics including the skewness, kurtosis, wave steepening factor, number of zero crossings and the Morfey-Howell nonlinearity indicator. Contours of these metrics in the (x, r)-plane reveal that the process of nonlinear acoustic wave steepening is absent within the measurement range considered. That, in combination with the findings from the aforementioned scaling model, provides confidence in stating that the detection of significant cumulative nonlinear waveform distortions in common laboratory-scale (range-restricted) environments is practically impossible. It is thus precluded that

observed shock-structures are the consequence of nonlinear wave steepening over distance. As a final note, it is advocated that when the Morfey-Howell indicator is used as an investigative tool for the presence of cumulative nonlinear waveform distortions, it must be applied as a multi-point indicator along spatial paths along which the sound travels in an ensemble-averaged fashion. Only when the statistical nature of the source is known to be purely Gaussian, the indicator can be applied as a single-point indicator. However, this is not applicable to jets, since the statistical nature of the noise sources are unknown.

7.2 Crackle emitted by high-speed jets

Several methods were pursued to quantify acoustic shock-structures in the sound field of the experimental Mach 3 jet. The absence of any cumulative nonlinear steepening effects in the measurement range (§ 7.1) implied that acoustic shock-structures are generated by *local* mechanisms in, or in close vicinity to, the jet's hydrodynamic region and that they can be classified as *crackle*. Some believe that the separation between the hydrodynamic region and acoustic region of a jet is equivalent to the separation identified by rotational and irrotational flow. The research on crackle was motivated by the fact that (1) it is perceived as the most annoying component of jet noise, (2) no unique measures of crackle exist, and (3) significant reductions in jet noise will be achieved when crackle can be controlled. Considering the second point, only a few statistical metrics have been applied to pressure waveforms in the past with an attempt to assess the existence of crackle. Shortcomings of

using these ensemble-averaged metrics are that they do not solely weight the waveform's shock content, but rather take the total waveform into consideration. This acts as a factor of noise in the quantification process. Henceforth, crackle is better quantified by studying the shock content.

A shock detection algorithm (SDA) was developed to detect shock fronts in the acoustic pressure waveforms. The algorithm was based on two user defined thresholds of the temporal pressure derivative (pressure rise time) and the pressure jump across the shock (shock strength). At first, the average shapes of the waveforms associated with crackle were obtained by ensemble-averaging all instances where shock-structures had been identified using the SDA. Shocks are close to being point-symmetric around the shock front (defined as the median time between pressure minima and maxima) at shallow angles to the jet axis and have rounded pressure minima and maxima. At angles near the Mach cone edge, the pressure maxima become more sharp and are indicative of less pronounced shock relaxation effects. It was concluded that classifying the shock-structures identified outside of the Mach cone as being crackle is highly questionable. Furthermore, within the Mach cone, the average number of shocks per second did not vary along radial lines of constant polar angle ϕ with a focal point residing in the region of most intense sound generation ($x = 17.5$ D_j). And so, the crackling structures travel efficiently in the sense that they do not disappear due to relaxation within the measurement range. Trends of temporal shock instances (arrival times) were subsequently studied. Like the average number of shocks per second, PDF's of the 1^{st}-order

intermittence are independent of the position on each of the radial lines A-G. The revealed modal behavior of the time instances provides evidence that shock-structures appear to be present in groups of multiple shocks. It was postulated that physical mechanisms leading to these modal observations are related to different families of curved wave fronts that form fringe patterns. Suggestions for future improvements in the detection and quantification of temporal shocks are itemized as follows.

- Currently, the SDA is based on a fixed rise time (the ratio of the two user defined thresholds, $\Delta t_s = 0.0540$ ms). However, from studies by Pierce [64] that are reviewed in the work of McInerny & Ölçmen (2005) [46], it became apparent that for stationary weak shocks (ones that propagate without a change in shape), the rise times are related to the jumps in pressure. And so, the SDA shock selection criteria can be adapted to reflect this dependence.

- Wavelet-based time-frequency analyses are used throughout the literature for shock detection [66, 1]. In this research, the wavelet power spectra are used secondary to the SDA to reveal spectral signatures of crackle. In future work, wavelet-based SDA can provide extra confidence in the correctness of shock detection.

- Various concepts explaining the temporal shock intermittencies were addressed in a preliminary fashion (§ 6.3.2). Synchronized measurements

of shock-structures (acoustic pressure) and pressure or velocity measurements in the hydrodynamic region of the jet (preferably spatially extensive) are believed to shed more light on these ideas. Furthermore, future work with analytical models encompassing the propagation of wave fronts can be insightful to reveal the true physical mechanisms of how these crackle-inducing structures manifest themselves in the sound field. Wave packet modeling (appendix A) appears to be a promising technique, especially when a sequence of wave packets is superposed, each having a unique axial wave number and pressure amplitude envelope.

A spectral measure of the level of crackle was considered by using wavelet-based time-frequency analyses. By employing the wavelet transform of acoustic waveforms, acoustic pressure spectra are generated as function of time. Thereafter, the time-frequency energy distribution is used to detect the unique spectral content associated with the shock fronts identified by the SDA, this is denoted as the shock spectrum. In order compute a practically significant measure, laboratory-scale spectra are scaled to an equivalent full-scale scenario at first. Secondly, spectra are A-weighted to account for the relative loudness perceived by the human ear at different frequencies within the audible range. The absolute increase of spectral sound energy between the global jet noise spectrum and the shock spectrum is independent of outward distance along radial lines and complies with the findings of constant temporal characteristics along the radial paths with constant polar angle ϕ. The increase in sound energy is quantified as the percentage energy gain from the

global pressure spectrum to the shock spectrum. This energy-based metric is postulated to be an appropriate metric for the perception of crackle since it provides the correct spatial trends: crackle is perceived dominantly at shallow angles and gradually becomes less pronounced at larger angles. Suggestions for future work on the spectral measures of crackle are itemized below.

- In order to conclude that energy-based quantification of crackle is relevant for the perception of crackle, a psycho-acoustic study involving blind jury trials has to be performed. The subjectiveness of crackle plays an important role in a quantitative measures of ones ability to reduce jet noise.

- On a final note, crackle and cumulative nonlinear distortions are most likely related. Findings suggest that crackle is not the consequence of cumulative nonlinear waveform distortions. However, cumulative effects can aid in the effectiveness of crackle, meaning that these effects prevent early relaxation of crackling structures, which therefore enhance the amplitude and perception of crackle.